Journal of Fluorine Chemistry 188 (2016) 185–190

Contents lists available at ScienceDirect

Journal of Fluorine Chemistry

journal homepage: www.elsevier.com/locate/fluor

Synthesis and NMR investigation of 2D nanocrystals of the LaF_3 doped by SrF_2

Larisa B. Gulina[a,*], Max Schäfer[b], Alexei F. Privalov[b], Valeri P. Tolstoy[a], Igor V. Murin[a], Michael Vogel[b]

[a] Institute of Chemistry, Saint Petersburg State University, 199034, 7/9 Universitetskaya nab., St. Petersburg, Russia
[b] Institut für Festkörperphysik, Technische Universität Darmstadt, D-64289 Darmstadt, Germany

ARTICLE INFO

Article history:
Received 23 June 2016
Received in revised form 15 July 2016
Accepted 16 July 2016
Available online 18 July 2016

Keywords:
Inorganic fluorides
LaF_3
SrF_2
HF
2D nanocrystals
Microtubes
NMR diffusometry
Ionic mobility
Gas–solution interface

ABSTRACT

Nanostructured superionic conductor LaF_3 doped by SrF_2 is obtained in the first time using the synthesis at the solution–gas interface. The product composition $La_{1-x}Sr_xF_{3-x}$ ($0 < x \leq 0.16$) was analyzed using SEM, FT-IR, XRD and EPM. It consists of nanosheets aggregated in microtubes. The SrF_2 content is varied from 2 mol% to 16 mol%. XRD analysis indicates tysonite crystal structure, which is still preserved up to 1000 K. NMR diffusometry has shown a significant enhancement of the diffusion coefficient, which is at least one order of magnitude higher than for undoped nanosized LaF_3 and about 3 orders of magnitude higher than for bulk LaF_3 at temperatures around 800 K.

1. Introduction

Lanthanum fluoride is an important material for optics [1,2], luminescence [3,4], sensors [5,6], biomedicine [7], and solid state ionics [8–12]. LaF_3 with the tysonite crystal structure possess superionic fluorine conductivity at high temperatures, which is governed by the disordering in the anionic sublattice. Doping of LaF_3 with SrF_2 enhances the ionic mobility significantly. The highest ionic conductivity was found for (3–5) mol% SrF_2. It is up to two orders of magnitude higher than in pure LaF_3 [13,14]. Several methods have been applied to obtain doped LaF_3: single crystals can be grown by Bridgman or Czochralski technique [15], ceramics can be obtained by hot pressing [16], thin films can be achieved by spin coating [17], vacuum deposition [18] or by layer-by-layer synthesis [19,20].

Strategies for the fabrication of materials are very important to improve their properties. In the past decade a lot of attention was paid to the methodology of the synthesis of tubular micro- and nanostructures due to their enhanced properties and potential applications related to their special morphology [21–26]. Recently, an innovative Gas–Solution Interface Technique (GSIT) was successfully applied to synthesize the well-known inorganic materials with the tubular morphology [27–32]. The interaction between cations from solution of salts and gaseous reagent by GSIT plays an important role in this type of synthesis. In particular the reaction between aqueous solution of lanthanum salt and gaseous HF leads to the formation of a film composed of two dimensional LaF_3 nanocrystals. Drying the film leads to a formation of microtubes [30]. The fluorine dynamics in this nanosized LaF_3 was found to be about two orders of magnitude higher, than in bulk [32]. To enhance the ionic conductivity of LaF_3 further, it seems to be promising to apply GSIT to obtain heterovalent doped materials.

In this work we apply GSIT to synthesize nanosized LaF_3 doped with different amounts of SrF_2. In analogy to proceeding our previous studies on nanosized and doped LaF_3 [32–39], the fluorine mobility of the doped LaF_3 nanocrystals is studied by NMR diffusometry. The results are compared with undoped nanocrystalline LaF_3 (obtained by GSIT) and with bulk LaF_3 [33].

2. Results and discussion

2.1. $La_{1-x}Sr_xF_{3-x}$ ($0 < x \leq 16$) layer formation by GSIT

As a result of the interaction of gaseous HF with the surface of a solution of mixed $LaCl_3$ and $SrCl_2$ a transparent thin film was

* Corresponding author.
E-mail address: l.gulina@spbu.ru (L.B. Gulina).

http://dx.doi.org/10.1016/j.jfluchem.2016.07.006
0022-1139/

formed. When transferred on the surface of support and dried at room temperature this film rolls into a microtube. The SEM investigation (Fig. 1) shows that the morphology of the film is determined by the relative concentration of the salts in the mixed solution. When only a small amount of strontium salt is added, the synthesized film is not dense having voids between the arrays of 2D nanosheets (Fig. 1*a,b*). The void space in the film decreases with increasing concentration of $SrCl_2$ (Fig. 1*c–e*). A film synthesized from the solution with maximal concentration of $SrCl_2$ (Fig. 1*e*) has a structure almost free of voids.

By electron probe microanalysis (EPMA) it is revealed that the concentration of elements in the synthesized product is not proportional to that in the solution (Fig. 2). Specifically, with increasing $SrCl_2$ salt concentration above 0.01 mol/l the content of Sr^{2+} in $La_{1-x}Sr_xF_{3-x}$ ($0 < x \leq 0.16$) film stills nearly unchanged. The highest SrF_2 concentration is about 16 mol%.

X-ray diffraction patterns for $La_{1-x}Sr_xF_{3-x}$ obtained by GSIT with dopant concentrations of 5 mol%, 13 mol% and 16 mol% are shown in Fig. 3. One can see a series of diffraction peaks assigned to the crystal planes of LaF_3 with its tysonite structure [ICDD PDF # 00-032-0483]. No further peaks related to other compounds are presented.

In our opinion, the difference of the solubility-product constant between SrF_2 and LaF_3 leads to the lanthanum fluoride with the tysonite-type phase initially formed at the interface. In according with [40] the solubility limits SrF_2 in LaF_3 were 2–15 mol% in dependent on production method and temperature. In GSIT synthesis conditions the highest SrF_2 content in tysonite was about 16%.

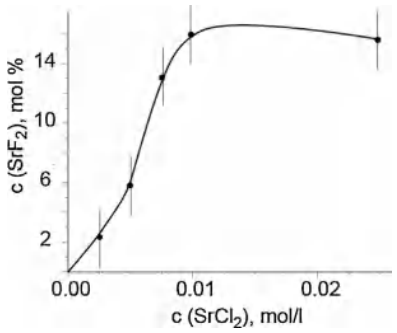

Fig. 2. Dependence of the SrF_2 content in nanosized $La_{1-x}Sr_xF_{3-x}$ ($0 < x \leq 0.16$) on the concentration of $SrCl_2$ salt in the mixed solution. The $LaCl_3$ concentration was 0.05 mol/l.

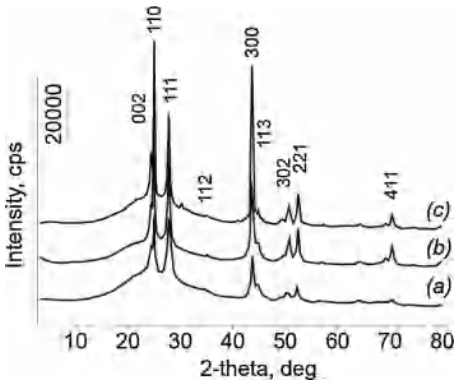

Fig. 3. X-ray diffraction patterns for $La_{1-x}Sr_xF_{3-x}$ with different SrF_2 contents *(a)* 5 mol%; *(b)* 13 mol%; *(c)* 16 mol%.

2.2. Synthesis and characterization of $La_{95}Sr_{0.05}F_{2.95}$ microtubes

For the investigation of diffusion coefficients we prepared the sample with the composition $La_{0.95}Sr_{0.05}F_{2.95}$ using GSIT. As can be seen from Fig. 4, the rolled tubes of $La_{0.95}Sr_{0.05}F_{2.95}$ have a diameter of about 70 μm and a length up to 2 mm. The SEM images show (Fig. 5) that the tube walls are consisting of ordered arrays of 2D nanocrystals oriented perpendicular to the wall surface. The tube wall has a thickness of about 0.5 μm and consists of densely packed (10–12) nm thick 2D crystals. On the inner side the wall density is lower as on the outer side (Fig. 5).

EPMA (Fig. 6) has shown the absence of remaining chlorine atoms from the aqueous solution of $LaCl_3$ and $SrCl_2$. The element composition of the tubes consists only of La, Sr and F atoms. The resulted ratio of Sr/La is 1/19 which corresponds to $La_{0.95}Sr_{0.05}F_{2.95}$.

The FT-IR spectrum of the $La_{0.95}Sr_{0.05}F_{2.95}$ sample (Fig. 7) display an absorption band at 335 cm^{-1} which can be attributed to La-F valence vibrations [41]. The bands at 3400 cm^{-1} and 1640 cm^{-1} are related to valence and to deformational oscillations of the O—H bonds of remaining water molecules respectively [42].

Fig. 8 shows XRD patterns of $La_{0.95}Sr_{0.05}F_{2.95}$ *a*) after the synthesis and *b*) after annealing at 1000 K. One can see a series of diffraction peaks well assigned to the crystal planes of LaF_3 with the tysonite structure [ICDD PDF # 00-032-0483]. No impurities are presented. The lattice parameters of $La_{0.95}Sr_{0.05}F_{2.95}$ obtained by Rietveld analysis were found as follows: space group $P^{-}3c1$; $a = 7.18415$; $c = 7.3553$ that are nearly to the parameters of undoped tysonite. Therefore the Sr^{+2} ions are uniformly incorporated into the host lattice of LaF_3. The resolution of the X-ray data was not sufficient to permit an accurate analysis of occupation of the La site by Sr for such a low doping content. After annealing at 1000 K the crystallinity is enhanced (Fig. 8*b*). Diffraction peaks from the

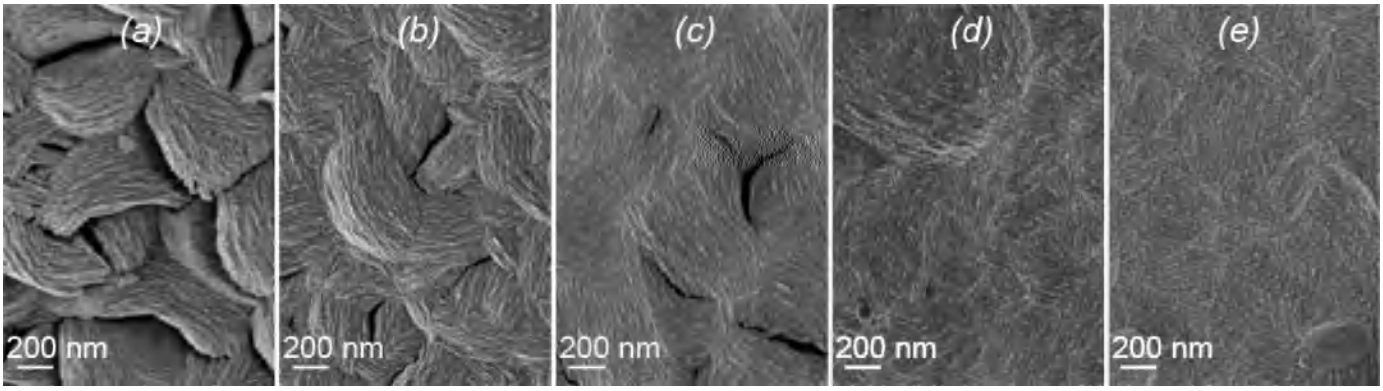

Fig. 1. SEM images of the films, synthesized from a mixed solutions of salts with 0.05 mol/l $LaCl_3$ and different concentrations of $SrCl_2$: *(a)* 0.00125 mol/l; *(b)* 0.0025 mol/l; *(c)* 0.005 mol/l; *(d)* 0.01 mol/l; *(e)* 0.025 mol/l.

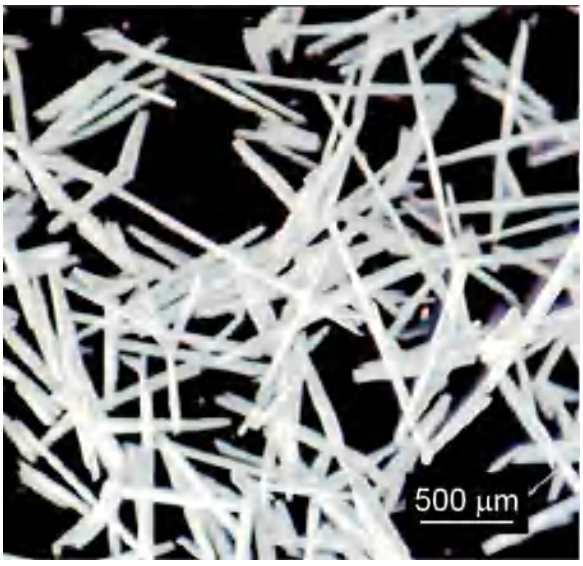

Fig. 4. Optical microscope image of $La_{0.95}Sr_{0.05}F_{2.95}$ tubes.

products of possible oxidation of the tysonite structure are not visible.

2.3. Fluorine dynamics from NMR data

Translational motion of fluorine ions in nanosized $La_{0.95}Sr_{0.05}F_{2.95}$ is studied by SFG NMR diffusometry. Due to the fact that the experiment probes diffusion on length scales from 100 nm to 1000 nm, geometrical restrictions of the nanosheets for motion perpendicular to the planes lead to an effective diffusion which can be treated as two dimensional (Eq. (1) in Experimental). In principle, additional geometrical restrictions along the sheets could lead to a time dependence of the resulting diffusion coefficient that could be lower for longer diffusion times and, thus, diffusion length, e.g. when defects in the sheet structure result in obstacles against the ionic diffusion on the experimental length scale. To determine whether our results are time independent we carry out stimulated echo measurements at various mixing times t_m (see Experimental). The data are fitted simultaneously using Eq. (1) multiplied by a factor for spin-spin relaxation. The Hahn echo and the stimulated echo amplitudes as a function of the evolution time τ for various t_m are presented in Fig. 9.

The curves are well fitted by the model of 2D diffusion. When the diffusion coefficients have no time dependence, after extraction of the relaxation terms one can create a single muster curve $S(q^2t)$ from the set of stimulated echo data (Fig. 9). In Fig. 10 we see that the decays indeed collapse into a single muster curve at all studied temperatures. Hence the decay of the master curve is determined by the diffusion coefficient only. Altogether, on the accessible time scales no evidence for a time dependence of the resulting diffusion coefficients can be found in the studied temperature range.

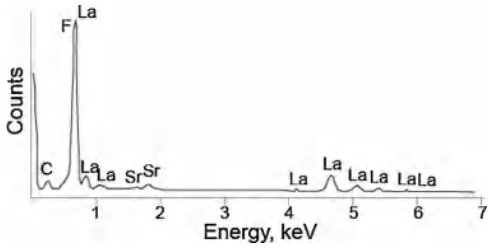

Fig. 6. EPMA spectrum of $La_{0.95}Sr_{0.05}F_{2.95}$ obtained by GSIT.

The results on diffusion coefficients are presented in Fig. 11 for doped nanosized LaF_3 in comparison with published data for undoped nanosized [32] and for bulk LaF_3 [33] as an Arrhenius plot. For all samples the dynamics can be well described by an Arrhenius law in the presented temperature range. The doped nanosized LaF_3 shows diffusion coefficients that are about three orders of magnitude higher than for undoped bulk LaF_3 and about one order of magnitude higher than for undoped nanosized LaF_3 at temperatures around 800 K. At lower temperatures the difference is even higher. The activation energy for bulk LaF_3 is 1.16 eV. For undoped nanosized LaF_3 it is 0.72 eV and for doped nanosized LaF_3 it is 0.31 eV. Thus we can conclude that below 700 K the nanosized doped sample $La_{0.95}Sr_{0.05}F_{2.95}$ possesses the highest ionic mobility known from the LaF_3 type ionic conductors [33].

3. Conclusion

It is shown that the thin layer of LaF_3 doped by SrF_2 ($0 < x \leq 0.16$) can be obtained by the synthesis at the gas–solution interface via the interaction between the mixture of aqueous solutions of $LaCl_3$ and $SrCl_2$ salts with gaseous HF. The amount of SrF_2 in the layer is controlled by concentration of strontium salt in initial solution and can be varied up to 16 mol%. The layers are built up from densely packed 2D nanocrystals, and the packing density depends on the synthesis conditions. The thickness of the 2D nanocrystals is about (10–12) nm. After drying the layers roll into microtubes, having a diameter of about (70–100) μm and a length up to 2 mm. The synthesized material has the crystal structure of tysonite. Up to 1000 K the tysonite structure remains.

NMR diffusometry has shown significant enhancement of the diffusion coefficients which are about one order of magnitude higher than for the undoped nanosized LaF_3 and about 3 orders of magnitude higher than for the bulk LaF_3. The nanosized $La_{0.95}Sr_{0.05}F_{2.95}$ shows the lowest activation energy of 0.31 eV in the temperature range from 625 K to 925 K.

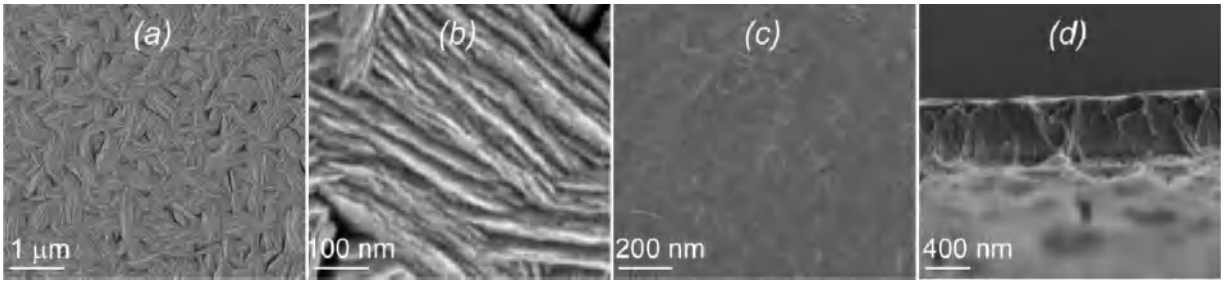

Fig. 5. SEM images of a $La_{0.95}Sr_{0.05}F_{2.95}$ tubular wall: *(a)* and *(b)* show the view from inside (different magnification); *(c)* outside view; *(d)* side view.

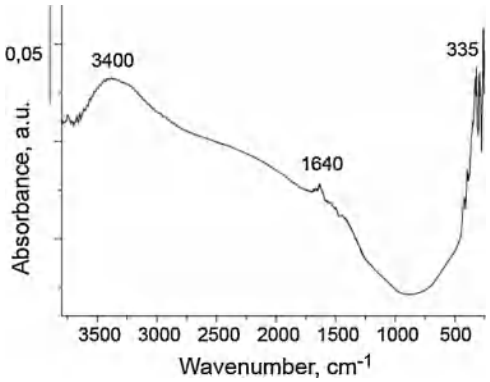

Fig. 7. FT-IR spectrum of a $La_{0.95}Sr_{0.05}F_{2.95}$ sample placed on a single-crystal silicon substrate.

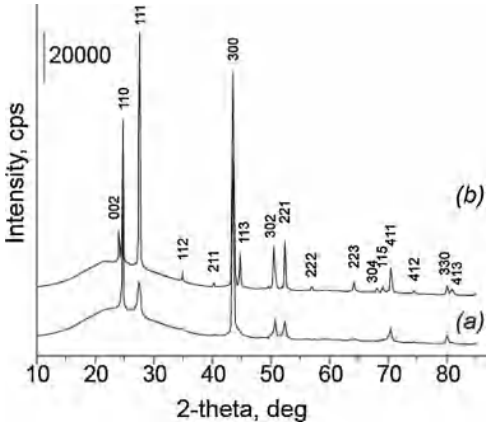

Fig. 8. X-ray diffraction patterns of $La_{0.95}Sr_{0.05}F_{2.95}$ sample as synthesized (*a*) and after annealing at 1000 K (*b*).

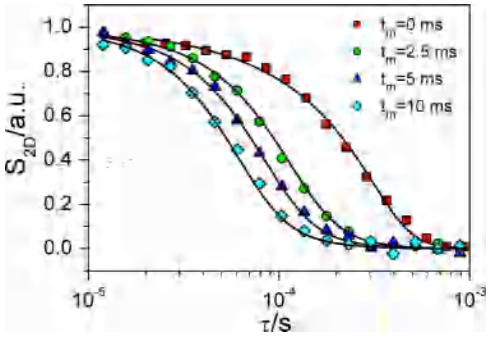

Fig. 9. Hahn echo ($t_m = 0$) and stimulated echo attenuation for various mixing times t_m at $T = 775$ K. The lines are fits using Eq. (1).

Nanosized material on the basis of doped LaF_3 obtained using GSIT is promising for all applications typical for solid state ionics.

4. Experimental

4.1. Synthesis

$LaCl_3$ (chemically pure) and $SrCl_2$ (extra pure) salts and 40% hydrofluoric acid provided by Vekton were used as reagents. Aqueous solutions were made using Milli-Q high purity water with a resistivity higher than 18 MΩ/cm. For the investigation of film

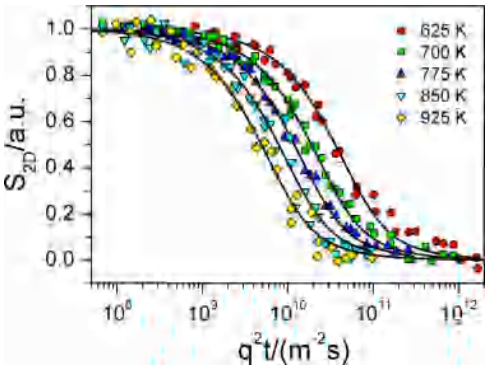

Fig. 10. Master curves for the echo decay at various temperatures.

formation peculiarities at the interface the weighed quantity of $SrCl_2$ was added to solution of 0.05 mol/l $LaCl_3$ in H_2O so that the concentration of $SrCl_2$ salt varies from 0.00125 mol/l to 0.025 mol/l.

The nanosized LaF_3 doped with SrF_2 was prepared via Gas–Solution Interface Technique (GSIT) [31]. For this purpose the mixed $LaCl_3$ and $SrCl_2$ salts solution was poured into a flat teflon vessel, than located into a hermetically sealed teflon lined chemical reactor and treated by gaseous HF during 30 min at room temperature. For the NMR investigation the sample was synthesized from a mixed solution with 0.045 mol/l $LaCl_3$ and 0.005 mol/l $SrCl_2$.

The film formed on the solution surface was transferred carefully onto the surface of pure distilled water and left for 10 min in order to remove the excess of reagent solution. After the procedure has been repeated twice, the film was transferred to the silicon wafer surface and dried at room temperature. The wafer was washed in acetone to remove organic impurities originated in environment and etched for 10 min in "piranha" solution (mixture of H_2O_2 and concentrated H_2SO_4 in the volume ratio of 3:7) with simultaneous ultrasonic cleaning (60 W) to prepare a hydrophylic surface and then rinsed thoroughly in water. During drying the films roll into microtubes.

4.2. Characterization

For structure and composition analysis we used SEM, FT-IR, XRD, EPMA and optical microscopy. The formation of microtubes was registered using a LCD digital optical microscope. The morphology was investigated using scanning electron microscopy (Zeiss EVO-40EP or Supra VP-40). The chemical composition and the Sr/La ratio was determined by EPMA using a scanning electron microscope equipped with an INCA 350 Energy EDX analyzer (Oxford Instruments). For the SEM and EPMA investigations the as-

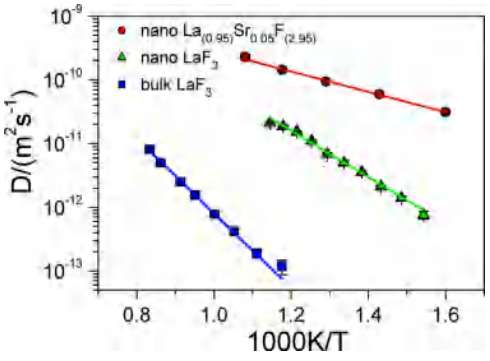

Fig. 11. Arrhenius plot of fluorine self-diffusion coefficients for doped nanosized, undoped nanosized and bulk LaF_3.

prepared microtubes were placed on carbon conductive tape. Infrared spectra were obtained on a Brucker Vertex 70 infrared spectrometer. To have a high signal-to-noise ratio, each IR spectrum was accumulated after 64 successive scans obtained at a spectral resolution of 4 cm^{-1}. X-ray powder diffraction was performed on diffractometer (Bruker D2 Phaser) equipped with Cu Kα X-ray source. For investigation of the thermal stability the sample was placed in a quartz-line test tube, heated to 1000 K with rate of 5 K/min, annealed at 1000 K during 1 h and slowly cooled to room temperature during 8 h.

4.3. Dynamics

To analyze the fluorine dynamics we performed NMR diffusometry in a static magnetic field gradient (SFG) [43] in the temperature range from 625 K to 925 K. A field gradient of g = 73 T/m is produced by a specially designed superconducting magnet with an antisymmetric arrangement of field coils. The experiments were performed at the Larmor frequency of 156 MHz, the 90° pulse length was 0.6 μs. A high temperature probe with micro furnace was used [44]. To measure diffusion coefficients a three pulse stimulated echo sequence for various mixing times t_m and a two pulse Hahn echo sequence were applied. The periods of de- and re-phasing are denoted as the evolution times τ [45]. For the stimulated echo sequence the magnetization storage time after the second RF pulse is given by the mixing time t_m. For the case of $t_m >> \tau$ the mixing time t_m can be approached as the diffusion time. In the case of the Hahn echo the diffusion occurs during τ. The echo decay for all experiments can be described by the same Eq. (1) whereby t_m is equal to zero for the Hahn echo.

For data analysis one has to consider the structural peculiarities, because the ion motion is restricted by the geometry of the nanosheets. SFG NMR diffusometry is sensitive for translational motion of fluorine ions on a mesoscopic length scale typically 100 nm–1000 nm, while the thickness of the sheets is only about 10 nm. Therefore this technique is not sensitive to diffusion in the direction perpendicular to the sheet plane and is sensitive to diffusion along the sheet plane. Therefore we can treat the diffusion as two dimensional.

The echo attenuation for two dimensional diffusion S_{2D} results by a powder averaged projection of the inclined sheet planes on the gradient direction over all polar angles θ weighted by $\sin\theta$ [45]. Without the relaxation terms the echo amplitude can be described by:

$$S_{2D} = \int_0^{\pi} \exp\left(-q^2 Dt \sin^2\theta\right) \sin\theta d\theta \Big/ \int_0^{\pi} \sin\theta d\theta = \int_0^1 \exp\left(-q^2 Dt\left(1-x^2\right)\right) dx \quad (1)$$

Where D is the self-diffusion coefficient, $t = 2\tau/3 + t_m$, and $q = \gamma g \tau$ is a generalized scattering vector [43] given by the product of the fluorine gyromagnetic ratio γ, the field gradient g and the evolution time τ.

Acknowledgements

The study was supported by Russian Science Foundation (grant 16-13-10223). The XRD research was carried out in the X-ray Diffraction Centre of SPbSU. The SEM study was carried out by the Nanotechnology Centre of SPbSU.

References

[1] S. Fujihara, K. Tokumo, Chemical processing for inorganic fluoride and oxyfluoride materials having optical functions, J. Fluorine Chem. 130 (2009) 1106–1110.
[2] A.J. Stevenson, H. Serier-Brault, P. Gredin, M. Mortier, Fluoride materials for optical applications: single crystals, ceramics, glasses, and glass–ceramics, J. Fluorine Chem. 132 (2011) 1165–1173.
[3] D. Chen, L. Liu, P. Huang, M. Ding, J. Zhong, Z. Ji, Nd3+-sensitized Ho3+ single-band red upconversion luminescence in core–shell nanoarchitecture, J. Phys. Chem. Lett. 6 (2015) 2833–2840.
[4] D. Chen, L. Lei, X.J. Xu, A. Yang, Y. Wang, Abnormal size-dependent upconversion emissions and multi-color tuning in Er3+-doped CaF2–YbF3 disordered solid-solution nanocrystals, Nanotechnology 24 (2013) 085708.
[5] A.A. Vasiliev, D.Y. Godovskiy, V.N. Bezmelnitsyn, V.S. Gazkov, F-ion conducting composite material for chemical sensors based on LaF_3 and polytetrafluoroethylene, J. Fluorine Chem. 58 (1992) 286.
[6] J.W. Fergus, The application of solid fluoride electrolytes in chemical sensors, Sens. Actuators B 42 (2) (1997) 119–130.
[7] R. Lv, S. Gai, Y. Dai, F. He, N. Niu, P. Yang, Surfactant-free synthesis, luminescent properties, and drug-release properties of LaF_3 and $LaCO_3F$ hollow microspheres, Inorg. Chem. 53 (2014) 998–1008.
[8] J. Schoonman, Fluorine solid electrolytes: fundamentals and applications, J. Fluorine Chem. 35 (1987) 153–154.
[9] F. Gschwind, G. Rodriguez-Garcia, D.J.S. Sandbeck, A. Gross, M. Weil, M. Fichtner, N. Hörmann, Fluoride ion batteries: theoretical performance, safety, toxicity, and a combinatorial screening of new electrodes, J. Fluorine Chem. 182 (2016) 76–90.
[10] C. Rongeat, M. Anji Reddy, R. Witter, M. Fichtner, Solid electrolytes for fluoride ion batteries: ionic conductivity in polycrystalline tysonite-type fluorides, ACS Appl. Mater. Interfaces 6 (2014) 2103–2110.
[11] V. Trnovcová, R.M. Zakalyukin, N.I. Sorokin, D. Lezal, P.P. Fedorov, E. Illeková, M. Ozvoldová, A. Skubla, B.P. Sobolev, Physical properties of multicomponent fluoride glasses for photonic and superionic applications, Ionics 7 (2001) 456–462.
[12] A. Kessler, R. Höger, I.V. Murin, Ion transport in LaF3 at low temperatures, Mater. Res. Bull. 16 (1981) 1185–1188.
[13] V. Trnovcová, P.P. Fedorov, I. Furár, Fluoride solid electrolytes containing rare earth elements, J. Rare Earths 26 (2008) 225–232.
[14] E.A. Krivandina, Z.I. Zhmurova, B.P. Sobolev, T.M. Glushkova, D.F. Kiselev, M.M. Firsova, A.P. Styrkova, Optical properties of crystals of $La_{1-x}Sr_xF_{3-x}$ solid solutions ($0 \le x \le 0.13$) with the tysonite structure, Crystallogr. Rep. 43 (1998) 85–89.
[15] N.I. Sorokin, M.V. Fominykh, E.A. Krivandina, Z.I. Zhmurova, B.P. Sobolev, O.I. Lyamina, Ion transport in the anion-deficient nonstoichiometric phases $La_{0.95}(Ba_{1-x}Sr_x)_{0.05}F_{2.95}$ ($0 \le X \le 1$), Phys. Solid State 40 (1998) 604–607.
[16] N.I. Sorokin, A.N. Smirnov, P.P. Fedorov, B.P. Sobolev, Superionic fluoride ceramics RF_3 and $R_{0.95}Sr_{0.05}F_{2.95}$ (R = La, Ce Pr, Nd) prepared by hot pressing, Russ. J. Electrochem. 45 (2009) 606–608.
[17] L. Zhang, M. Anji Reddy, M. Fichtner, Development of tysonite-type fluoride conducting thin film electrolytes for fluoride ion batteries, Solid State Ionics 272 (2015) 39–44.
[18] N.I. Sorokin, E.F. Sudakova, E.A. Krivandina, B.P. Sobolev, Thin films of the $La_{0.95}Sr_{0.05}F_{2.95}$ fluoride-ionic semiconductor: impedancemetry with platinum electrodes, Russ. J. Electrochem. 35 (1999) 223–227.
[19] B.S. Zhuchkov, V.P. Tolstoy, I.V. Murin, Synthesis of ScF_3, LaF_3 nanolayers and $nLaF_3$-$mScF_3$ multinanolayers at the surface of silicon by successive ionic layer deposition method, Solid State Ionics 101–103 (1997) 165–170.
[20] Y.S. Milovanov, V.A. Skryshevsky, V.P. Tolstoy, L.B. Gulina, I.V. Gavrilchenko, G. V. Kuznetsov, Photoluminescence of porous silicon coated by SILD method with LaF_3 nanolayers, Curr. Appl. Phys. 13 (2013) 1625–1629.
[21] A.A. Krasilin, A.M. Suprun, E.V. Ubyivovk, V.V. Gusarov, Morphology vs. chemical composition of single Ni-doped hydrosilicate nanoscroll, Mater. Lett. 171 (2016) 68–71.
[22] H. Zhang, J. Peng, Y. Shen, X. Yu, F. Zhang, J. Mei, B. Li, L. Zhang, Hybrid microtubes of polyoxometalate and fluorescence dye with tunable photoluminescence, Chem. Commun. 48 (2012) 4462–4464.
[23] Q.A.H. Al-Naser, J. Zhou, G. Liu, L. Wang, Investigation and characterization of ZnO single crystal microtubes, Mater. Charact. 114 (2016) 97–102.
[24] A.A. Krasilin, V.V. Gusarov, Energy of formation of chrysotile nanotubes, Russ. J. Gen. Chem. 84 (2014) 2359–2363.
[25] V. Luchnikov, O. Sydorenko, M. Stamm, Self-rolled polymer and composite polymer/metal micro- and nanotubes with patterned inner walls, Adv. Mater. 17 (2005) 1177–1182.
[26] S.V. Golod, V.Y. Prinz, P. Wägli, L. Zhang, O. Kirfel, E. Deckhardt, F. Glaus, C. David, D. Grützmacher, Freestanding SiGe/Si/Cr and SiGe/Si/SixNy/Cr microtubes, Appl. Phys. Lett. 84 (2004) 3391–3393.
[27] V.P. Tolstoy, L.B. Gulina, New way of As_2S_3 microtubules preparation by roll up thin films synthesized at the air-solution interface, J. Nano Electron. Phys. 5 (2013).
[28] V.P. Tolstoi, L.B. Gulina, Ozone interaction with manganese acetate solution. Formation of $H_xMnO_2 \cdot nH_2O$ layers and microtubes based on them, Russ. J. Gen. Chem. 83 (2013) 1635–1639.
[29] V.P. Tolstoy, L.B. Gulina, Synthesis of birnessite structure layers at the solution-air interface and the formation of microtubules from them, Langmuir 30 (2014) 8366–8372.
[30] L.B. Gulina, V.P. Tolstoy, Reaction of gaseous hydrogen fluoride with the surface of lanthanum chloride solution to form $LaF_3 \cdot nH_2O$ film and microtubes thereof, Russ. J. Gen. Chem. 84 (2014) 1472–1475.

[31] L.B. Gulina, V.P. Tolstoy, I.A. Kasatkin, Y.V. Petrov, Facile synthesis of LaF_3 strained 2D nanoparticles and microtubes at solution-gas interface, J. Fluorine Chem. 180 (2015) 117–121.
[32] L.B. Gulina, M. Schäfer, A.F. Privalov, V.P. Tolstoy, I.V. Murin, Synthesis of LaF_3 nanosheets with high fluorine mobility investigated by NMR relaxometry and diffusometry, J. Chem. Phys. 143 (2015) 234702.
[33] F. Fujara, D. Kruk, O. Lips, A.F. Privalov, V. Sinitsyn, H. Stork, Fluorine dynamics in LaF_3-type fast ionic conductors—combined results of NMR and conductivity techniques, Solid State Ionics 179 (2008) 2350–2357.
[34] M.A. Denecke, W. Gunßer, A.V. Privalov, I.V. Murin, NMR and XAS study on doped LaF3, Solid State Ionics 52 (1992) 327–331.
[35] A.F. Privalov, I.V. Murin, H.M. Vieth, Superionic conductors with tysonite structure: evidence for a distribution of motional correlation times from 19F-NMR data, Ionics 2 (1996) 319–322.
[36] A.F. Privalov, I.V. Murin, Ion-motion disorder in a tysonite superionic conductor from 19F NMR data, Phys. Solid State 41 (1999) 1482–1485.
[37] A.F. Privalov, A. Ceniani, F. Fujara, H. Gabriel, I.V. Murin, H.M. Vieth, The distribution of motional correlation times in superionic conductors: 19F nuclear magnetic resonance of tysonite-like LaF_3, J. Phys. Cond. Matter 9 (1997) 9275–9287.
[38] A.F. Privalov, H.M. Vieth, I.V. Murin, Ionic motion in the LaF_3 superionic conductor studied by 19F NMR with homonuclear decoupling, J. Phys. Chem. Solids 50 (1989) 395–398.
[39] V.V. Sinitsyn, O. Lips, A.F. Privalov, F. Fujara, I.V. Murin, Transport properties of LaF_3 fast ionic conductor studied by field gradient NMR and impedance spectroscopy, J. Phys. Chem. Solids 64 (2003) 1201–1205.
[40] M. Yoshimura, K.J. Kim, S. Sōmiya, Revised subsolidus phase diagram of the system SrF_2–LaF_3, Solid State Ionics 18 (1986) 1211–1215.
[41] V.P. Tolstoy, I.V. Chernyshova, V.A. Scryshevsky, Handbook of Infrared Spectroscopy of Ultrathin Films, Wiley-Interscience, New Jersey, 2003.
[42] K. Nakamoto, Infrared and Raman Spectra of Inorganic and Coordination Compounds. Part A: Theory and Applications in Inorganic Chemistry, 5th ed., Wiley, New York, 1997.
[43] B. Geil, Measurement of translational molecular diffusion using ultrahigh magnetic field gradient NMR, Concepts Magn. Reson. 10 (1998) 299–321.
[44] A.F. Privalov, O. Lips, Low-cost high-temperature NMR probe head, Appl. Magn. Reson. 22 (2002) 597–600.
[45] P.T. Callaghan, Principles of Nuclear Magnetic Resonance Microscopy, Oxford University Press Inc., New York, 1991.